Binary-fluid-mixture convection with low-frequency modulated heating

B. L. Smorodin[1,*] and M. Lücke[2]
[1]*Perm State University, 614990 Perm, Russia*
[2]*Institut für Theoretische Physik, Universität des Saarlandes, Postfach 151150, D-66041 Saarbrücken, Germany*
(Received 23 April 2010; published 15 July 2010)

The response behavior of binary fluid convection to low-frequency temporal modulation of the heating is studied for the case of a negative Soret coupling between temperature and concentration gradients. Numerical simulations using a finite difference method are carried out for ethanol-water mixtures subject to realistic boundary conditions. We study in particular the response when the Rayleigh number periodically drops below the saddle node in the bifurcation diagram of convective solutions under stationary heating, i.e., into a regime where convection would die out in the absence of modulation. Quasiperiodic traveling waves, several different periodic traveling waves, and synchronously modulated patterns with fixed spatial phase are found as stable solutions depending on parameters. The symmetry properties of the different periodic traveling waves are discussed. Anomalous variations of the mixing behavior relative to advection are observed and explained. Lateral and temporal Fourier decompositions are used together with other diagnostic tools to analyze the complex bifurcation and spatiotemporal properties that are caused by the interplay of modulated heating, nonlinear advection, Soret induced gradients, and mixing of the fluid.

DOI: 10.1103/PhysRevE.82.016310 PACS number(s): 47.20.Ky, 47.20.Lz, 47.54.−r

I. INTRODUCTION

Self-organization and pattern formation phenomena appear in many nonlinear dissipative systems that are driven sufficiently far away from thermal equilibrium [1]. One example of such systems is convection in binary miscible fluids such as, e.g., ^{3}He-^{4}He or ethanol-water. It shows a rich and interesting variety of different patterns and it displays a wide range of phenomena related to instabilities, transport, bifurcations, and self-organization with complex spatiotemporal behavior.

Compared to convection in homogeneous fluids such as, e.g., pure water or pure ethanol the spatiotemporal properties of binary mixtures are rather complex. That is related to concentration gradients which are generated via thermodiffusion—i.e., the Soret effect—by externally imposed and by internal temperature gradients. These concentration gradients influence the buoyancy, i.e., the driving force for convective flow. The latter in turn mixes the two components of the binary mixture and therefore advectively redistributes concentration. This nonlinear advection gets in developed convective flow typically much larger than the smoothing by linear diffusion: the Péclet numbers measuring the strength of advective concentration transport relative to diffusion are easily $\mathcal{O}(1000)$. In this case the concentration balance is strongly nonlinear giving rise to large variations of the concentration field with narrow boundary layers. The momentum and heat balances, on the other hand, show weakly nonlinear behavior close to onset as in homogeneous fluids with smooth and basically harmonic variations of the velocity and temperature fields as of the critical modes.

In the absence of the thermodiffusive Soret coupling between temperature and concentration gradients any initial concentration deviation from the mean diffuses away and influences no longer the balances of the other fields. Hence, the feedback interaction between (i) the Soret generated concentration variations, (ii) the resulting changes in the buoyancy, and (iii) the strongly nonlinear advective transport and mixing causes binary mixture convection to be rather complex with respect to its spatiotemporal properties and its bifurcation behavior. In the case of modulated heating the complexity of the interplay between these processes increases even further as will be elucidated in this paper.

We investigate here convection in binary fluid mixtures in the case of negative Soret coupling $\psi<0$ between temperature and concentration gradients [2,3] when the lighter component migrates to cooler regions thereby stabilizing the density stratification in the quiescent laterally homogeneous conductive fluid state. Then the above described feedback interaction generates oscillations of mixture. In fact the buoyancy difference in regions with different concentrations was identified already in [4] as the cause for traveling-wave (TW) convection.

In contrast to steady convection oscillatory behavior in binary mixtures appears in a rather large variety: as transient growth of convection at supercritical heating, in spatially extended nonlinear TW and standing wave (SW) solutions that branch out of the conductive state via a common Hopf bifurcation, in spatially localized TW states, and in various types of fronts [1,5–23]. The oscillations appear with different characteristics. For instance, the Hopf frequency ω_H of the oscillatory instability of the quiescent fluid characterizes the linear stage of fast oscillating convective perturbations. On the other hand, the upper solution branch of the stable strongly nonlinear TWs that have bifurcated backward out of the conductive state is characterized by much smaller frequencies. Under modulation such systems can demonstrate complex resonance phenomena [24,25].

The influence of time-dependent gravitational accelerations or vibrations on the onset of Rayleigh-Bénard convection was studied in [26]. The linear stability problem for the single component system was reduced to the damped

*bsmorodin@yandex.ru

Mathieu equation. It was shown that high-frequency vibrations can increase the stability of the quiescent state. Finite frequency vibrations, on the other hand, can destabilize the quiescent state by resonance phenomena. The effect of modulating the temperature of the horizontal boundaries on the threshold for the onset of convection in a horizontal layer of a homogenous fluid was studied in Refs. [27–29]. In the quiescent basic state the temperature modulation drives heat waves that propagate diffusively between the boundaries of the layer.

The convective instability of a pure fluid under vibrations or under a modulated temperature gradient can be related to two types of critical disturbances that are in general the first that get undamped: for a synchronous response the oscillation period of the convective disturbances coincides with the period of the external modulation. In the case of a subharmonic response the period of the latter is twice as large as the modulation period. The influence of temporal modulation on pattern formation and nonlinear dynamics in pure liquids was investigated experimentally [30] and theoretically [31]. A Lorenz-like model of the hydrodynamic equations was used in these investigations.

In this work we consider spatially extended convection patterns consisting of straight rolls as they appear in narrow rectangular and annular channels. These structures can efficiently be described in the two-dimensional vertical x-z cross section in the middle of the channel perpendicular to the roll axes ignoring variations in the y-axis direction. Furthermore, these convection structures have relevant phase gradients only in the x direction thus causing effectively one-dimensional patterns [32]. For such structures we explore the effect of modulating the heating rate, i.e., the forcing mechanism that causes convection in the first place.

Modulated heating with a frequency Ω that is large compared to the TW frequencies under stationary driving was investigated in [24]. There, depending on parameters, the following variety of the convective response behavior was found: (i) synchronously oscillating rolls with a fixed spatial phase, (ii) quasiperiodic TWs in which basically only the amplitude is modulated, (iii) more strongly modulated TWs where also the phase velocity gets modulated, and (iv) frequency locked subharmonic SWs that get stabilized by the modulation. All in all, high-frequency modulation with relative modulation amplitudes of 20% around the mean heating rate extended the existence range of these oscillating structures to lower mean Rayleigh numbers in comparison to the case of stationary thermal driving.

Here, we show why the response characteristics for low-frequency modulation—being partly more complex—differ from the high-frequency case. To that end we perform numerical simulations of strongly nonlinear convection in binary mixtures with negative Soret coefficients. In particular we elucidate the spatiotemporal behavior and the bifurcation properties of different convective structures under temporal modulation with amplitudes of 20% around the mean. Then, the Rayleigh number periodically drops below the saddle location of TWs under stationary heating, i.e., into a regime where convection would die out in the absence of modulation.

The paper is organized as follows. In Sec. II we describe the problem and the governing equations. In Sec. III we give a brief summary of the unmodulated case and under large-frequency modulation before presenting in Sec. IV our results in the presence of low-frequency modulation. The last section is devoted to concluding remarks.

II. SYSTEM

We consider a horizontal plane layer of a binary fluid mixture that is placed in the earth's gravitational field with the acceleration g. The layer is bounded by rigid perfectly heat conducting and impervious parallel planes located at $z=0$ and $z=h$. Thus, h is the thickness of the layer. The fluid might be a mixture of water with the lighter component ethanol at a mean mass concentration $\bar{C}$. The temperature T_u of the upper boundary is fixed. The temperature T_l that is imposed at the lower boundary is modulated harmonically with angular frequency Ω according to

$$T_l(t) = T_u + \Delta T(1 + \delta \sin \Omega t). \tag{2.1}$$

The mean temperature difference is ΔT and its relative modulation amplitude is δ. We use T_u as the reference temperature $\bar{T}$ and we consider the (small) variations of the fluid density ρ due to temperature and concentration variations to be governed by the linear thermal and solutal expansion coefficients $\alpha=-\frac{1}{\rho}\frac{\partial \rho}{\partial T}$ and $\beta=-\frac{1}{\rho}\frac{\partial \rho}{\partial C}$, respectively. Both are positive for ethanol-water.

A. Equations

To describe convection in this binary fluid mixture we use the balance equations for mass, momentum, heat, and concentration in the Oberbeck-Boussinesq approximation which read in nondimensional form [21,33,34]

$$\boldsymbol{\nabla} \cdot \mathbf{v} = 0, \tag{2.2a}$$

$$\frac{\partial \mathbf{v}}{\partial t} + (\mathbf{v} \cdot \boldsymbol{\nabla})\mathbf{v} = -\boldsymbol{\nabla} p + \sigma \nabla^2 \mathbf{v} + \sigma R(T + C)\mathbf{e}_z, \tag{2.2b}$$

$$\frac{\partial T}{\partial t} + (\mathbf{v} \cdot \boldsymbol{\nabla})T = \nabla^2 T, \tag{2.2c}$$

$$\frac{\partial C}{\partial t} + (\mathbf{v} \cdot \boldsymbol{\nabla})C = L\nabla^2(C - \psi T). \tag{2.2d}$$

Here, $\mathbf{v}$ is the velocity field, p is the pressure, and $\mathbf{e}_z$ is the unit vector directed upward. T and C are scaled (cf. below) deviations of temperature and concentration from $\bar{T}$ and $\bar{C}$, respectively. The field equations (2.2) contain the Rayleigh number R characterizing the thermal driving of the fluid and three other parameters describing the physical properties of binary fluid mixture: the Prandtl number σ, the Lewis number L, and the separation ratio ψ,

$$R = \frac{g\alpha \Delta T h^3}{\nu \kappa}, \quad \sigma = \frac{\nu}{\kappa}, \quad L = \frac{D}{\kappa},$$

$$\psi = -\frac{\beta\kappa_T}{\alpha\bar{T}} = S_T\bar{C}(1-\bar{C})\frac{\beta}{\alpha}. \tag{2.3}$$

Here, ν is the kinematic viscosity, κ is the thermal diffusivity, and D is the concentration diffusion constant of the mixture, while $k_T=\bar{T}\bar{C}(1-\bar{C})S_T$ is the thermodiffusion coefficient [33] and S_T is the Soret coefficient. Furthermore, the following scales have been used in Eqs. (2.2): length, h; time, h^2/κ; velocity, κ/h; temperature, ΔT; concentration, $\alpha\Delta T/\beta$; and pressure, $\rho\kappa^2/h^2$.

We solved the field equations (2.2) for two-dimensional roll convection with axes oriented in the y direction. To that end we introduced the stream function Ψ and the vorticity φ which are connected to the velocity field in the following way:

$$\mathbf{v} = \left(\frac{\partial\Psi}{\partial z}, 0, -\frac{\partial\Psi}{\partial x}\right), \quad \varphi = (\boldsymbol{\nabla}\times\mathbf{v})_y. \tag{2.4}$$

Then the partial differential equations (2.2) are transformed into

$$\varphi = \nabla^2\Psi, \tag{2.5a}$$

$$\frac{\partial\varphi}{\partial t} + \frac{\partial\Psi}{\partial z}\frac{\partial\varphi}{\partial x} - \frac{\partial\Psi}{\partial x}\frac{\partial\varphi}{\partial z} = \sigma\nabla^2\varphi - \sigma R\frac{\partial(T+C)}{\partial x}, \tag{2.5b}$$

$$\frac{\partial T}{\partial t} + \frac{\partial\Psi}{\partial z}\frac{\partial T}{\partial x} - \frac{\partial\Psi}{\partial x}\frac{\partial T}{\partial z} = \nabla^2 T, \tag{2.5c}$$

$$\frac{\partial C}{\partial t} + \frac{\partial\Psi}{\partial z}\frac{\partial C}{\partial x} - \frac{\partial\Psi}{\partial x}\frac{\partial C}{\partial z} = L\nabla^2(C-\psi T). \tag{2.5d}$$

1. Boundary conditions

The horizontal boundaries at $z=0,1$ are taken to be of no slip ($\mathbf{v}=0$) and impervious, so that there

$$\Psi = 0, \quad \frac{\partial\Psi}{\partial z} = 0, \quad \frac{\partial C}{\partial z} - \psi\frac{\partial T}{\partial z} = 0. \tag{2.6}$$

The temperatures at the boundaries are

$$T(z=0) = 1+\delta\sin\Omega t, \quad T(z=1) = 0. \tag{2.7}$$

Laterally we impose periodic boundary conditions, $f(x,z,t)=f(x+\lambda,z,t)$, on all fields $f=\Psi,\varphi,T,C$ with $\lambda=2$ throughout the paper.

2. Parameters

In this paper we consider mixtures with $L=0.01$, $\sigma=10$, and $\psi=-0.25$. This set of parameters is characteristic for and easily experimentally realizable with ethanol-water mixtures. The wave number of the convection rolls is $k=\pi$. It is close to the critical one and close to the one that one typically observes for oscillatory convection rolls at negative ψ, say, in narrow annular containers. The relative amplitude of the temperature modulation (2.1) of the lower boundary is $\delta=0.2$. We consider small modulation frequencies, namely, $\Omega=0.2\omega_H$, $\Omega=0.1\omega_H$, and $\Omega=0.01\omega_H$. Here, $\omega_H=11.246$ is the Hopf frequency at the onset of oscillatory convection with wave number $k=\pi$ for static heating.

3. Conductive state

In the conductive state, i.e., when the fluid is motionless the temperature $T_{cond}(z,t)$ and the concentration $C_{cond}(z,t)$ fields satisfy the one-dimensional diffusion equations,

$$\frac{\partial T_{cond}}{\partial t} = \frac{\partial^2 T_{cond}}{\partial z^2}, \tag{2.8}$$

$$\frac{\partial C_{cond}}{\partial t} = L\left(\frac{\partial^2 C_{cond}}{\partial z^2} - \psi\frac{\partial^2 T_{cond}}{\partial z^2}\right), \tag{2.9}$$

respectively, together with the boundary conditions (2.6) and (2.7). The conductive temperature distribution following from Eq. (2.8) is given by a superposition of a static linear profile and a damped heat wave propagating from the lower boundary into the fluid,

$$T_{cond}(z,t) = T^0_{cond}(z) + T^1_{cond}(z,t), \tag{2.10a}$$

$$T^0_{cond} = 1-z, \tag{2.10b}$$

$$T^1_{cond} = \delta\,\mathrm{Re}\left\{i\frac{\sinh[\alpha(z-1)]}{\sinh\alpha}e^{i\Omega t}\right\}, \quad \alpha=\sqrt{i\Omega}. \tag{2.10c}$$

The conductive concentration distribution resulting from Eq. (2.9) is determined by the temperature distribution (2.10) due to the thermal diffusion effect,

$$C_{cond}(z,t) = C^0_{cond}(z) + C^1_{cond}(z,t), \tag{2.11a}$$

$$C^0_{cond} = \psi\left(\frac{1}{2}-z\right), \tag{2.11b}$$

$$C^1_{cond} = \psi\delta\,\mathrm{Re}\left\{i\alpha\frac{\beta\cosh\alpha\cosh[\beta(z-1)] - \beta\cosh(\beta z) + \alpha\sinh[\alpha(z-1)]\sinh\beta}{(\alpha^2-\beta^2)\sinh\alpha\sinh\beta}e^{i\Omega t}\right\}, \quad \beta=\sqrt{iL\Omega}. \tag{2.11c}$$

Thus, both the temperature and concentration fields in the motionless mixture have a steady part and an oscillating part with zero mean. The steady part varies linearly in z. The part that oscillates harmonically in time with the modulation frequency Ω has an amplitude that varies linearly in δ. But it has a more complicated z dependence, the details of which depend on Ω. The oscillatory part of the concentration also depends on ψ and L; cf. Eq. (2.11c) for $C^1_{cond}(z,t)$. Snapshots of this quantity at different times during the modulation period are shown for the case of a large modulation frequency $\Omega=\omega_H$ in Fig. 1(a) and two smaller ones, $\Omega=0.1\omega_H$ and $\Omega=0.01\omega_H$, in Figs. 1(b) and 1(c), respectively.

When modulating with the large frequency $\Omega=\omega_H$ the thermodiffusion processes at our set of parameters do not have time enough to create substantial deviations of the concentration distribution from its static mean $C^0_{cond}(z)$ in Fig. 1(a). Thus, in this case the oscillatory contribution $C^1_{cond}(z,t)$ does not influence the dynamics of convection significantly.

At low frequencies, say, $\Omega<0.2\omega_H$, the temperature addition $T^1_{cond}(z,t)$ and therefore the total temperature distribution $T_{cond}(z,t)$ are practically linear functions of z at each moment of the driving period. However, the concentration additions $C^1_{cond}(z,t)$ still depend strongly on frequency. In the range $L\omega_H<\Omega<\omega_H$ they have nonlinear z profiles.

Modulation with a small frequency, say, $\Omega=0.01\omega_H$ as in Fig. 1(c) leads to contributions of $C^1_{cond}(z,t)$ to the concentration distribution of several percent near the boundaries. Thus, for example, at $z=0$ and $z=1$ one has $C^1_{cond}\simeq 0.135C^0_{cond}$ at time $\Omega t=\frac{3}{8}2\pi$ for our modulation amplitude of $\delta=0.2$.

4. Solution method

For solving the system of equations (2.5) in the general case of $\Psi\neq 0$ an alternating-direction implicit scheme is used with central differences for the spatial derivatives and one-sided right differences for the time derivatives. This is a finite difference method of second order. The stream function was determined with an iterative method of successive overrelaxation at each time step. Typically, a state of relaxed finite amplitude convective oscillations obtained at a particular set of parameters was used as the initial condition for a run at another set of parameters.

B. Diagnostic tools

To measure the intensity of the heating we use the reduced Rayleigh number $r=R/R^0_c$, where R^0_c is the critical Rayleigh number for onset of pure-fluid convection with the critical wave number k^0_c. Linear stability theory predicts $R^0_c=1707.8$ and $k^0_c=3.116$. However, to compare our finite difference numerical results presented in this paper with experimental, analytical, or numerical ones we scale R by the threshold $R^0_c=1701.5$ of our numerical code. Most of the calculations are executed using grids of 47×31 nodes. A further mesh refinement to 82×61 nodes does not provide a significant improvement in the evaluation of oscillation characteristics and shows no relevant differences.

For the modulation (2.1) of the temperature at the lower boundary the time-dependent reduced Rayleigh number,

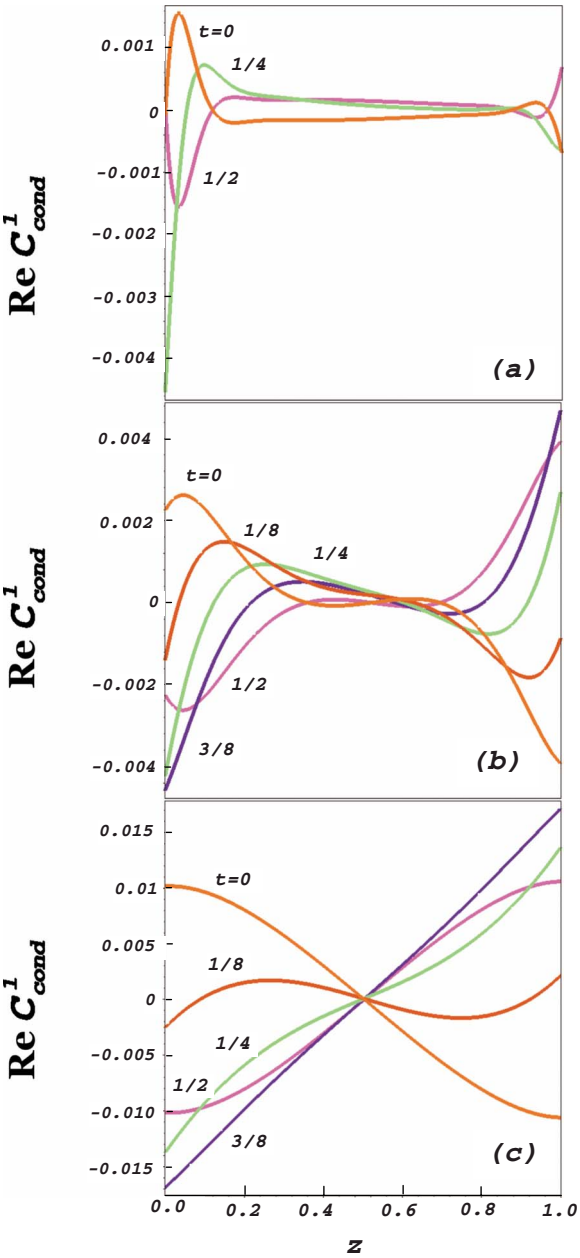

FIG. 1. (Color online) Conductive concentration variations in the case of temperature modulation of the lower boundary. Shown are snapshots of the z dependence of the term $C^1_{cond}(z,t)$ (2.11c) entering into the conductive concentration distribution (2.11a). The snapshot times 0, 1/8, 1/4, 3/8, and 1/2 that label the curves in the figures refer to fractions of the respective modulation cycle. Frequencies are (a) $\Omega=\omega_H=11.246$, (b) $\Omega=0.1\omega_H$, and (c) $\Omega=0.01\omega_H$. Parameters are $\delta=0.2$, $L=0.01$, and $\psi=-0.25$.

$$r(t)=r[1+\delta\sin(\Omega t)], \tag{2.12}$$

is modulated around a mean value r with relative amplitude δ. To monitor the convection intensity we use the maximum and the minimum of the vertical flow field in the x-z cross section perpendicular to the roll axes,

$$w_{max}(t)=\max_{x,z} w(x,z,t), \tag{2.13a}$$

$$w_{min}(t) = \min_{x,z} w(x,z,t), \tag{2.13b}$$

as well as the time evolution of w at a fixed position x_0, z_0.

We also consider running time averages of various quantities $f(t)$ over some time interval, in particular over a period of the modulation $\tau = 2\pi/\Omega$,

$$\langle f \rangle(t) = \frac{1}{\tau}\int_{t-\pi/2}^{t+\pi/2} f(t')dt', \tag{2.14}$$

as well as long-time averages,

$$\langle f \rangle = \frac{1}{\mathcal{T}}\int_0^{\mathcal{T}} f(t)dt, \tag{2.15}$$

with very large $\mathcal{T}$. The latter is used among others to determine the mean lateral velocity $\langle v_{ph} \rangle$ of the phase of w as measured by the time derivative of node locations of $w(x, z=1/2, t)$ at midheight of the fluid layer, $v_{ph} = dx_{(w=0)}/dt$. Thus,

$$\langle v_{ph} \rangle = [x_{(w=0)}(\mathcal{T}) - x_{(w=0)}(0)]/\mathcal{T}. \tag{2.16}$$

For all modulated TWs with lateral periodicity $\lambda = 2\pi/k$ we use the mean phase velocity $\langle v_{ph} \rangle$ (2.16) to identify

$$\langle \omega_{TW} \rangle = \langle v_{ph} \rangle k \tag{2.17}$$

as the mean frequency of a modulated TW. We also use the frequency ratio

$$Q = \Omega/\langle \omega_{TW} \rangle \tag{2.18}$$

as a diagnostic tool. In general Q is not a rational number. In that case one has a quasiperiodic modulated TW. For a periodic TW the frequency ratio $Q = m/n$ is the quotient of two integer numbers m and n. The set of periodic TWs contains the subharmonic one with $Q=2$ and also synchronous TWs with $Q=1$.

To elucidate the spatiotemporal complexities of the convective behavior and of the transitions between various regimes we have also studied lateral Fourier decompositions,

$$f(x,t) = f_0(t) + \mathrm{Re}\sum_{n=1}^{\infty} \hat{f}_n(t)e^{-inkx}, \tag{2.19}$$

of the fields at midheight position $z=1/2$. The behavior there is largely representative for all other z's.

Finally, we analyzed the time evolution of the spatial variance of the concentration field in the layer. To that end we monitored the mixing number of the concentration field,

$$M = \sqrt{\overline{C^2}/\overline{(C^0_{cond})^2}}. \tag{2.20}$$

Here, the overbar implies a spatial average over the layer. In the unmodulated ($\delta=0$) quiescent ($\mathbf{v}=0$) layer the Soret induced conductive concentration profile $C^0_{cond}(z)$ (2.11b) varies from $-\psi/2$ at the top boundary to $\psi/2$ at the bottom one with $\overline{(C^0_{cond})^2} = \psi^2/12$.

In the unmodulated conductive state one has $M=1$ by definition. In the modulated conductive state M depends on time with a maximum that grows with decreasing frequency and that is larger than 1: for example, $M_{max}(\Omega=\omega_H)=1.002$ but $M_{max}(\Omega=0.01\omega_H)=1.134$. However, when convection is present then the advective mixing reduces the mean square deviation $\overline{C^2}$ of the concentration—the better the fluid is mixed advectively the smaller is M coming closer to the limit $M=0$ for a perfectly mixed fluid.

III. STATIONARY HEATING AND MODULATION WITH LARGE FREQUENCY

In Sec. III A we give a brief overview of the main bifurcation and spatiotemporal properties of laterally extended convection states in the absence of modulation, $\delta=0$; cf. [5,20] for more details. Then, in Sec. III B a short synopsis of the effect of large-frequency modulation ($\delta=0.2$, $\Omega=\omega_H$) [24] is presented. Both these reviews serve to give the background on which we present our results for low-frequency modulation in Sec. IV.

A. Stationary heating

When increasing the heating quasistatically the onset of convection in the ethanol-water mixture occurs for our parameters via a Hopf bifurcation at the reduced Rayleigh number $r_{osc}=1.335$ with a Hopf frequency $\omega_H(k=\pi, r_{osc}) = 11.246$ according to linear stability theory. Our finite difference numerical method, on the other hand, yields $r_{osc} = 1.318$. Thin lines in Fig. 2(a) show for $\delta=0$ the bifurcation diagrams of maximal vertical flow velocity w_{max} versus r for the SW solution, the TW solution, and the stationary overturning convection (SOC) solution. The last solution branch is disconnected from the quiescent conductive state. The SW and the pair of the symmetry degenerated left and right traveling-wave solutions bifurcate backward out of the conductive state at r_{osc}.

When following the solution branches TWs gain stability in a saddle-node bifurcation at $r_S^{TW}=1.175$ while SWs remain unstable. For $r < r_S^{TW}$ convection in the unmodulated fluid layer damps out and the system goes to the conductive state. Only above r_S^{TW} stable, yet strongly nonlinear, TW convection exists. This stable TW solution branch ends at $r^*=1.36$ by merging with zero frequency in the SOC branch thereby transferring its stability to the SOC solution. In the interval $r_S^{TW} < r < r_{osc}$ an unstable TW solution branch exists which becomes weakly nonlinear when approaching the threshold r_{osc}.

There are not only quantitative but also significant qualitative structural differences—most predominant in the concentration field—between weakly and strongly nonlinear TWs. The isoconcentration lines of weakly nonlinear TW are open and the field looks almost harmonic. On the other hand, in strongly nonlinear TWs there exist well-mixed regions of almost constant concentration. They are surrounded by closed isolines and open ones meander between the closed isoline domains in a strongly anharmonic fashion.

The thin lines in Fig. 2(b) correspond to the bifurcation behavior of the frequency ω of the nonlinear SW and TW solutions for stationary heating, $\delta=0$. These frequencies are largest at the Hopf bifurcation threshold r_{osc}. There, one has $\omega_H=11.246$. Then, upon moving with increasing flow amplitude w_{max} along the solution branches in Fig. 2(a) the fre-

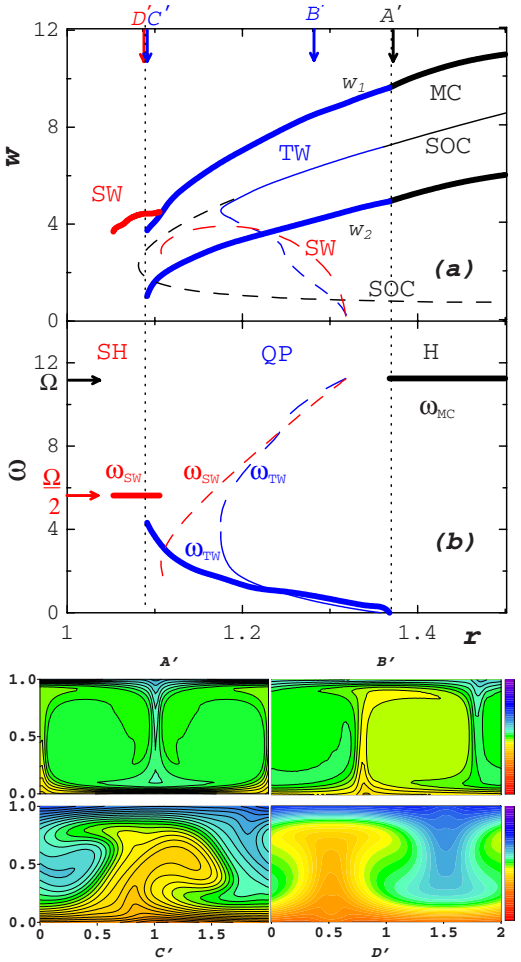

FIG. 2. (Color online) Bifurcation diagrams of laterally extended convective states with wave number $k=\pi$ in binary fluid mixtures as functions of the reduced Rayleigh number r. Thick lines refer to temperature modulation (2.1) of the lower boundary with relative amplitude $\delta=0.2$ and large frequency $\Omega=\omega_H=11.246$. Vertical dotted lines mark boundaries of quasiperiodic (QP) and harmonic (H) responses to modulation in the form of TWs and phase fixed modulated convection (MC), respectively. Under modulation the maximal vertical velocity $w_{max}(t)$ (2.13) oscillates between the thick lines labeled by w_1 and w_2, respectively, in (a). Thick lines in (b) denote the largest Fourier contribution in the frequency spectrum of the vertical velocity. Thin lines refer to (a) w_{max} and (b) the frequency of the reference states under stationary heating, $\delta=0$, with full (dashed) ones denoting stable (unstable) solutions. The insets below (b) show representative snapshots of the concentration distribution in the layer in the presence of temperature modulation for (A′) MC, (B′) amplitude modulated TW, (C′) amplitude and phase modulated TW, and (D′) SW. Their r values are indicated by arrows in (a). In the color online version the vertical color bars show the coding in the unmodulated conductive state with $C^0_{cond}(z)$ varying linearly from −0.125 at the bottom to 0.125 at the top for $\psi=-0.25$. Parameters are $L=0.01$, $\sigma=10$, and $\psi=-0.25$.

quency decreases. Thus, e.g., the TW frequency at the saddle, r_S^{TW}, has dropped already to $\omega_S^{TW}=3.88$. Continuing further—now with increasing r—along the upper TW solution branch of Fig. 2(a) the TW frequency decreases further until it reaches zero at r^* where the TW branch ends in a drift instability of the SOC branch.

B. Modulation with large frequency

Modulation of the thermal driving force for convection with a relative amplitude as large as $\delta=0.2$ generates a very rich response behavior even for a modulation frequency $\Omega=\omega_H$ that is large compared to the TW frequencies under stationary driving [24]. This is not really surprising since already the unmodulated convective states are strongly nonlinear with quite complex spatiotemporal behavior of the concentration field that is largely determined by strong advective transport.

For most of the r values shown in Fig. 2 the oscillation of the reduced Rayleigh number $r(t)$ (2.12) covers an interval from well below the lower existence limit of unmodulated nonlinear TWs at $r_S^{TW}=1.175$ to well above its upper existence limit at $r^*=1.36$. This changes the bifurcation diagram for the stationary case (thin lines in Fig. 2) into a form shown by thick lines in Fig. 2 for $\delta=0.2$, $\Omega=\omega_H$. For example, the maximal vertical flow velocity $w_{max}(t)$ (2.13) oscillates between the values w_2 and w_1 shown in Fig. 2. Stable SOC states become synchronously modulated convection (MC) which oscillates with frequency Ω and fixed spatial phase around the SOC solution for stationary heating. Insets A′, B′, C′, and D′ below the bifurcation diagrams of Fig. 2 show typical concentration distributions for (A′) modulated convection, (B′) a pure amplitude modulated TW, (C′) a phase modulated TW, and (D′) a SW.

In TW solutions under stationary heating the maximal vertical flow velocity is a constant but now it oscillates with the period of $r(t)$. In the TW B′ shortly below r^* basically only the amplitude is modulated. With decreasing r the TW phase velocity becomes modulated more and more as well (TW C′). Here, the mixing behavior of the concentration is very complex with open- and closed-streamline regions appearing as alternating. The existence range of these modulated TWs extends down to r values well below the saddle location r_S^{TW} of unmodulated TWs. Thus, modulation with $\delta=0.2$, $\Omega=\omega_H$ stabilizes TW convection.

At the lower end of the r range of modulated TWs there is a hysteretic transition to subharmonic SWs. These periodic states are frequency locked over a finite r interval to oscillate with half the modulation frequency. The modulation-stabilized SWs occur below the saddle r_S^{SW} of unstable unmodulated SWs. They are less nonlinear and—in particular with respect to their concentration field structure—closer to the quiescent conductive state than the highly nonlinear TWs.

IV. MODULATED HEATING WITH LOW FREQUENCY

In this paper we consider modulation with a relatively large modulation amplitude of $\delta=0.2$. Then, for most of the mean values $r=\langle r(t)\rangle$ that we have investigated here, the driving $r(t)$ (2.12) drops periodically below the saddle location r_S^{TW} below which unmodulated convection would decay into the conductive state. An important property among oth-

ers that then influences the response behavior of convection is the length of time over which $r(t)$ remains during the modulation cycle below r_S^{TW}. We consider here a "low-frequency" situation where $r(t)$ stays long enough subcritical, i.e., below r_S^{TW}, so that the TW flow amplitudes become small during part of the cycle. Under such conditions stable low-frequency modulated TWs exist only for $r > r_S^{TW}$ while large-frequency modulated TWs [24] exist also well below r_S^{TW}. Here, we investigate the frequency range $0.01\omega_H \leq \Omega \leq 0.2\omega_H$ in which we found qualitatively similar characteristics of such a low-frequency response.

Depending on the size of r this convective response is periodic or quasiperiodic in the form of a modulated TW or, at larger r, it is harmonic with the driving in the form of MC. But under low-frequency modulation we do not observe stable SWs as in the large-frequency case (cf. the thick lines in Fig. 2 representing subharmonic SWs). Before we elucidate the properties of the convective solutions in more detail in Secs. IV B and IV C we shortly want to discuss the question of the relevant time scales.

A. Time scales

Consider first the time scales for diffusive transport of momentum, heat, and concentration $(1/\sigma, 1, 1/L) = (0.1, 1, 100)$ and for vertical advection of these fields $1/w_{max}$, all expressed in units of the vertical thermal diffusion time h^2/κ. So, for flow intensities $w_{max} > 1$ that are typical for nonlinear convective states under stationary heating or large-frequency modulation concentration is advection dominated and is not smoothed diffusively while the converse is true for the velocity field: the balance equation for momentum is weakly nonlinear (as long as the rate for advective momentum transport is small compared to the diffusive transport rate), while the balance equation for concentration is strongly nonlinear with its Péclet number w_{max}/L being typically very large.

Furthermore, for our low-frequency modulation the period $\tau = 2\pi/\Omega$ is comparable to the decay time under stationary heating of a TW or of SW that is prepared to have as initial conditions saddle characteristics slightly below r_S^{TW} or r_S^{SW}. Under modulation such decay dynamics will take place when the driving $r(t)$ stays long enough below the saddle locations. Then $w_{max}(t)$ decreases to very small values in a significant part of the modulation period.

For modulation with $\Omega = 0.1\omega_H$ the period $\tau \simeq 5.6$ is larger than the momentum and heat diffusion times, so that the velocity and the temperature fields have enough time to be smoothed out diffusively. The behavior of the concentration field depends on the size of r; cf. the bifurcation diagram in Fig. 3. When $w_{max} > 1$ throughout the modulation cycle then the concentration field remains advection dominated. Such convective dynamics occurs when $r(t)$ does not remain too long below the saddle r_S^{TW}. On the other hand, when r is located only shortly above the lower end r_{min}^{TW} of the existence interval of stable modulated TWs, then the concentration field is advection dominated only in that part of the modulation cycle where $w_{max} > 1$; cf. further below. Then, thermodiffusion processes are most important in the other part of driving cycle in which $w_{max} < 1$.

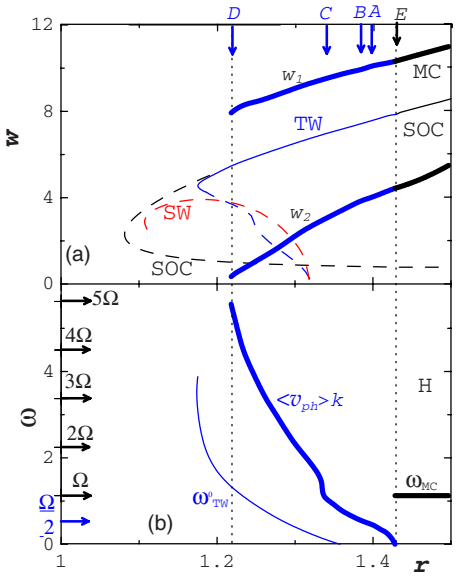

FIG. 3. (Color online) Bifurcation diagrams of laterally extended convective states with wave number $k = \pi$ in binary fluid mixtures as functions of the reduced Rayleigh number r. Thick lines refer to temperature modulation (2.1) of the bottom boundary with relative amplitude $\delta = 0.2$ and the low frequency $\Omega = 0.1\omega_H = 1.125$. Vertical dotted lines at $r_{min}^{TW} = 1.217$ and $r_{max}^{TW} = 1.430$ show the limits of the existence range of stable modulated TWs. MC identifies the range of harmonically responding phase fixed modulated convection. Under modulation the maximal vertical velocity $w_{max}(t)$ (2.13) oscillates between the thick lines in (a) labeled by w_1 and w_2, respectively. Thick lines in (b) denote the average TW frequency $\langle \omega_{TW} \rangle = \langle v_{ph} \rangle k$. Arrows labeled A, B, C, D, and E locate states that are discussed in the text. Thin lines referring to (a) the maximal vertical flow velocity and (b) the frequency for stationary heating, $\delta = 0$, are explained in the caption of Fig. 2. Parameters are $L = 0.01$, $\sigma = 10$, $\psi = -0.25$.

In the case of $\Omega = 0.01\omega_H$ the modulation period $\tau \simeq 56$ is of the same order as the concentration diffusion time, and advection can become very small during the part of the cycle where $r(t) < r_S^{TW}$. During these times also the balance equation for concentration is practically linear when its Péclet number w_{max}/L is very small.

B. Modulated traveling waves

Low-frequency temperature modulation shifts the boundaries $(r_{min}^{TW}, r_{max}^{TW})$ of the existence range of stable TWs upward in r: from $(r_S^{TW}, r^*) = (1.175, 1.361)$ for $\delta = 0$ to (1.217, 1.430) for $\delta = 0.2, \Omega = 0.1\omega_H$; cf. thick lines in Fig. 3. For $\Omega = 0.2\omega_H$ one has $(r_{min}^{TW}, r_{max}^{TW}) = (1.182, 1.415)$ and for $\Omega = 0.01\omega_H$ the range is (1.270, 1.434). So, for low-frequency modulation one has $r_{min}^{TW} > r_S^{TW}$, while for large-frequency modulation TWs exist well below the saddle location r_S^{TW} of unmodulated TWs. But, on the other hand, low-frequency modulated TWs exist well above the end r^* of the unmodulated TW solution branch, while under large-frequency modulation the upper end r_{max}^{TW} of the TW branch lies close to r^* [24].

1. Fourier spectra

The modulated TWs are in general quasiperiodic oscillatory convective states with two different characteristic frequencies: the external driving frequency Ω and the average frequency $\langle\omega_{TW}\rangle$ (2.17). In a narrow interval below r_{max}^{TW} the TWs are only amplitude modulated with almost constant phase velocities such that there, $v_{ph} \approx \langle v_{ph}\rangle$ at any time. But with decreasing r the modulation of the phase velocity increases. We first discuss the convective dynamics at driving parameters where not only the TW amplitudes but also the phase velocities are modulated significantly and where the concentration dynamics gets quite complex. This is already the case at the location marked by arrow A in Fig. 3.

The frequency spectrum of the vertical velocity $w(x_0, z=1/2, t)$ at $r=1.399$, i.e., at location A in the bifurcation diagram of Fig. 3 is shown in Fig. 4(a). It contains three major contributions: a main peak at $\langle\omega_{TW}\rangle$ and two secondary peaks at $\Omega \pm \langle\omega_{TW}\rangle$. The variation of $\langle\omega_{TW}\rangle$ with r is shown by the thick line in Fig. 3(b). It drops to zero at r_{max}^{TW}, beyond which the response range of MC begins while with decreasing r the frequency $\langle\omega_{TW}\rangle$ increases.

The structure of the Fourier spectrum is a consequence of the quadratic character of the nonlinear terms in Eqs. (2.5). Without modulation the convective system generates a TW with characteristic frequency ω_{TW}. The modulation of the heating changes this frequency into $\langle\omega_{TW}\rangle$ and, furthermore, it generates a temperature wave of frequency Ω. The heat balance equation contains the term $(\partial T_{cond}/\partial z)(\partial \Psi/\partial x)$ which generates new harmonics $\Omega \pm \langle\omega_{TW}\rangle$ in the temperature field. The related buoyancy force then produces in the fields of vorticity φ and velocity w corresponding oscillations. The further nonlinear interaction of two harmonics $\Omega + \langle\omega_{TW}\rangle$ and Ω restores back the TW frequency $\langle\omega_{TW}\rangle$. Hence, this harmonic being created in two different ways has the largest amplitude in the Fourier spectrum.

Higher Fourier harmonics in the evolution of $w(x_0, z=1/2, t)$ at frequencies

$$\omega = \pm \langle\omega_{TW}\rangle + m\Omega \tag{4.1}$$

with integer $m > 1$ are very small since the momentum balance equation is only weakly nonlinear. On the other hand, the frequency spectrum of the concentration wave contains significant anharmonicities as one can also infer from the spatial profiles of the C waves discussed in Sec. IV B 2.

With decreasing r the peaks in Fig. 4(a) at $\langle\omega_{TW}\rangle$ and $\Omega - \langle\omega_{TW}\rangle$ approach each other (as indicated by full arrows) since $\langle\omega_{TW}\rangle$ grows with decreasing r [cf. Fig. 3(b)]: the flow intensity and the advective mixing decrease, the Soret induced diffusive concentration gradients become less washed out, the resulting restoring force for oscillations increases, and thus $\langle\omega_{TW}\rangle$ grows. With increasing r, on the other hand, the peaks in Fig. 4(a) move as indicated by the dotted arrows.

The spectrum in Fig. 4(b) belongs to the subharmonically responding TW at $r=1.383$ (location B in Fig. 3) with $\langle\omega_{TW}\rangle = \Omega/2$. Here, the largest contribution to the Fourier spectrum is at $\Omega - \langle\omega_{TW}\rangle = \Omega/2$. We would like to emphasize that contrary to the large-frequency case where stable subharmonically responding SWs exist in a finite r interval there is no frequency locking here: the subharmonically responding TW exists only at one particular value of r.

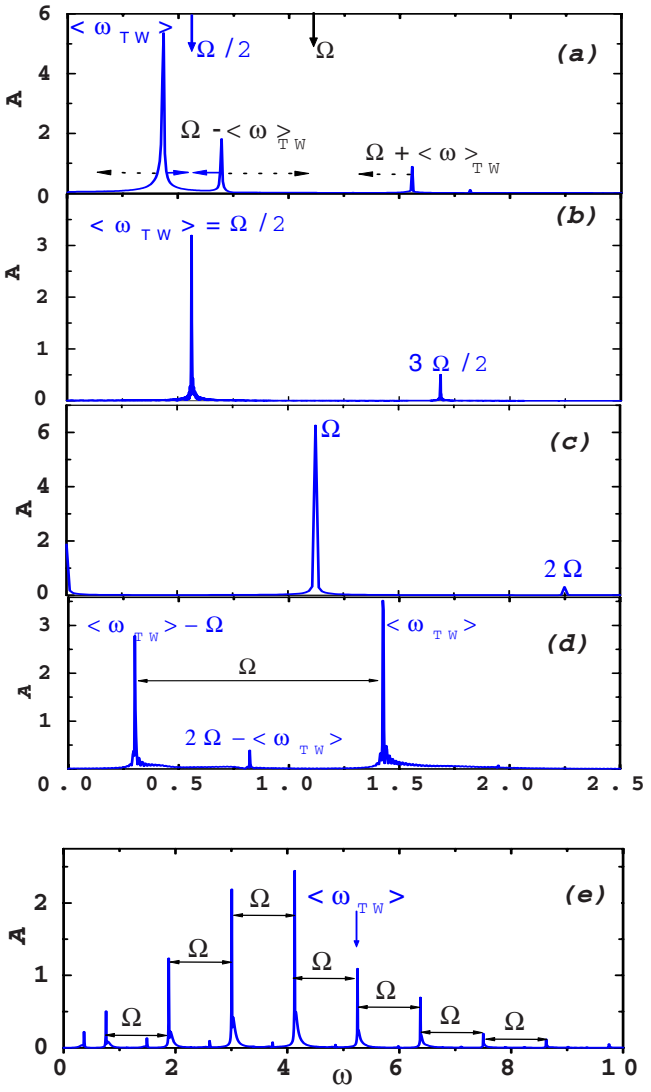

FIG. 4. (Color online) Fourier amplitudes A in arbitrary units in the spectrum of $w(x_0, z=1/2, t)$ versus frequency ω. (a) Amplitude and phase modulated TW at $r=1.399$ (arrow A in Fig. 3), (b) subharmonic TW at $r=1.383$ (arrow B in Fig. 3), (c) synchronous TW at $r=1.337$ (arrow C in Fig. 3), (d) modulated TW at $r=1.322$, and (e) strongly modulated TW at $r=1.222$ (arrow D in Fig. 3). Peaks labeled $\langle\omega_{TW}\rangle$ are characterized by the average phase velocity $\langle v_{ph}\rangle = \langle\omega_{TW}\rangle/k$. Full (dotted) horizontal arrows in (a) indicate how the peaks move when r decreases (increases) as a consequence of the variation of $\langle\omega_{TW}(r)\rangle$ shown in Fig. 3(b). Parameters are $\Omega = 0.1\omega_H = 1.125$, $\delta=0.2$, $L=0.01$, $\sigma=10$, and $\psi=-0.25$.

The spectrum in Fig. 4(c) corresponds to the harmonically responding TW at $r=1.337$ (location C in Fig. 3) with $\langle\omega_{TW}\rangle = \Omega$. Here, the largest contribution to the Fourier spectrum of this periodic convective state is at Ω. Note that there is also a sizable contribution at $\omega=0$ which appears due to nonlinear interaction of harmonics at $\Omega - \langle\omega_{TW}\rangle = 0$. So, in this harmonically modulated TW there is a stationary contribution to the flow field coming from the temporally averaged velocity $w(x,z,t)$.

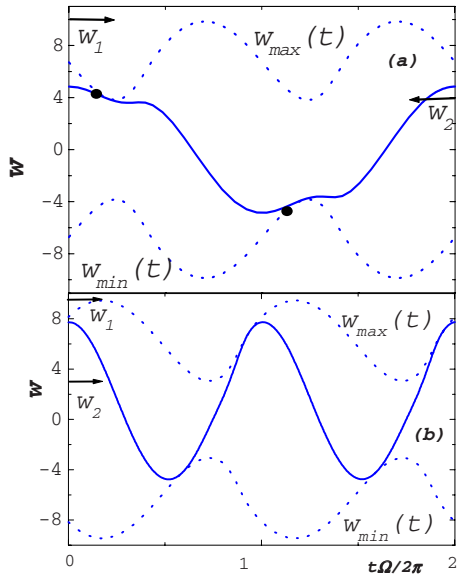

FIG. 5. (Color online) Time variation of the vertical velocity of periodically responding TWs: (a) subharmonic TW B in Fig. 3 and (b) synchronous TW C in Fig. 3. Thick lines show w at a fixed location $(x_0, z=1/2)$ and dotted lines show the minimum w_{min} and maximum w_{max} (2.13) in the whole layer. The oscillation range of the latter is indicated by w_1 and w_2. The plots cover two modulation cycles of $r(t)$. Thick dots in (a) identify times for snapshots of the concentration distribution shown in Fig. 6. Parameters are $\Omega = 0.1\omega_H = 1.125$, $\delta = 0.2$, $L = 0.01$, $\sigma = 10$, and $\psi = -0.25$.

Upon further decrease in r the average TW frequency $\langle\omega_{TW}\rangle$ grows beyond Ω. That brings new peaks in the spectrum at locations (4.1) that are lying below the one at $\langle\omega_{TW}\rangle$. Such a situation is shown in Fig. 4(d) where $\langle\omega_{TW}\rangle = 1.270\Omega$. One can see contributions at $\langle\omega_{TW}\rangle - \Omega$ and at $-\langle\omega_{TW}\rangle + 2\Omega$. Contributions of the form (4.1) that are lying on the high-frequency side of $\langle\omega_{TW}\rangle$ are smaller.

When, with further decreasing r, $\langle\omega_{TW}\rangle$ becomes larger than 2Ω, the structure of the Fourier spectrum becomes even more rich. In Fig. 4(e) we show the spectrum for the TW at $r = 1.222$ (arrow D in Fig. 3) near the lower end r_{min}^{TW} of the existence interval of modulated TWs. Its average frequency $\langle\omega_{TW}\rangle = 5.24$ is about 4.7 times larger than Ω and 12 times larger than that of TW A in Fig. 3(a). It contains on the low-frequency side sizable peaks down to a frequency of $\langle\omega_{TW}\rangle - 4\Omega$ and furthermore also a few peaks at $\langle\omega_{TW}\rangle + |m|\Omega$. Again the peak heights at low frequencies are typically larger than those at higher frequencies.

2. Flow behavior and concentration field

In this section we discuss the advective flow and its influence on the concentration distribution in the modulated TWs. We first consider the subharmonic TW (arrow B in Fig. 3) with $Q=2$ and the synchronous TW (arrow C in Fig. 3) with $Q=1$ before we discuss the strongly modulated and strongly anharmonic TW labeled D in Fig. 3 with $Q=0.214$.

For the first two we show the vertical velocity at midheight $z=1/2$ at a fixed lateral position x_0 in Fig. 5 as a function of time over two modulation periods by thick lines. The oscillations of $w_{max}(t)$ and of $w_{min}(t)$ (2.13) are indicated by dotted lines. They cover the ranges (w_2, w_1) and $(-w_2, -w_1)$, respectively. These extrema are also indicated in Fig. 3(a). Note that the instantaneous global extrema w_2 and w_1 are usually not localized at $x_0, z=1/2$.

It is interesting to note that the lateral variation of the flow in these modulated TWs remains largely harmonic as in the absence of modulation. Thus, the complete spatiotemporal behavior of w at midheight can reasonably well be captured by the first lateral Fourier mode $\hat{w}_1$ in expansion (2.19), so that

$$w\left(x, z=\tfrac{1}{2}, t\right) = \mathrm{Re}[\hat{w}_1(t)e^{-ikx}] \tag{4.2a}$$

is a good approximation. In Sec. IV C we show that the modulus of $\hat{w}_1(t) = |\hat{w}_1(t)|e^{i\varphi_1(t)}$ oscillates with frequency Ω between the extrema w_2 and w_1 which is well be captured by

$$|\hat{w}_1(t)| = \frac{w_1 + w_2}{2} + \frac{w_1 - w_2}{2}\sin(\Omega t + \alpha), \tag{4.2b}$$

with some constant α. The rate of change $\dot{\varphi}_1(t)$ of the phase, on the other hand, oscillates periodically around $\langle\omega_{TW}\rangle = \Omega/Q$ in these periodic TWs such that

$$\varphi_1(t) = \langle\omega_{TW}\rangle t + \Delta\varphi_1(t) \tag{4.2c}$$

increases by 2π within one period $2\pi/\langle\omega_{TW}\rangle$ of the TW. See Sec. IV C for further details.

Here, we want to show how one can understand with Eqs. (4.2) some of the spatiotemporal symmetry behavior of the periodic TWs with $Q \geq 1$. We found that subharmonically responding TWs with even $Q=2m$ show the time-shift symmetry

$$w(x,z,t) = -w(x,z,t + \pi/\langle\omega_{TW}\rangle), \tag{4.3}$$

whereas those with odd $Q=2m+1$ do not. The reason is that after half the TW period the exponential term $e^{i\varphi_1(t)}$ changes sign. But the modulus $|\hat{w}_1(t)|$ needs the time $2\pi/\Omega = 2\pi/(Q\langle\omega_{TW}\rangle)$ for its restoration. We checked that this time-shift symmetry of the vertical velocity holds not only at midheight but also at other z positions. Furthermore, one can understand with Eqs. (4.2) that at any fixed lateral position $x=x_0$ the time average $\langle w(x_0,t)\rangle$ over a period of the TW vanishes for periodic TWs with $Q \geq 2$ using simple forms for the periodic variation of the phase deviation $\Delta\varphi_1(t)$ from the mean phase growth in Eq. (4.2c). On the other hand, for $Q=1$ one sees in this way that $\langle w(x_0,t)\rangle$ is nonzero.

The evolution of the concentration field for the subharmonic TW at $r=1.382$ (arrow B in Fig. 3) with $Q=2$ is shown in Fig. 6 by two snapshots of C in the x-z plane. The snapshot times are separated by a period of the modulation. They are indicated by thick dots in Fig. 5(a). This TW propagates to the left.

With the phase velocity $1.187 < v_{ph} < 2.88$, being small compared to the extrema $w_2 = 3.88$ and $w_1 = 9.79$ of $w_{max}(t)$, this TW is a slow [35] strongly nonlinear state with strong advective mixing of the concentration field [5]: the difference between maximal and minimal C is much smaller than in the unmodulated conductive state; cf. the color bar on the right side of Fig. 6. Furthermore, there are very narrow

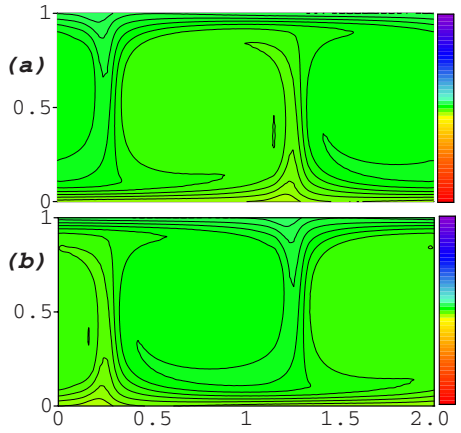

FIG. 6. (Color online) Snapshots of the concentration distribution in the subharmonically responding left propagating TW at $r=1.383$ (arrow B in Fig. 3). Snapshot times are identified by thick dots in Fig. 5(a). The time difference between (a) and (b) is $2\pi/\Omega$. In the color online version the vertical color bars show the coding in the unmodulated conductive state with $C^0_{cond}(z)$ varying linearly from −0.125 at the bottom to 0.125 at the top for $\psi=-0.25$. Parameters are $\Omega=0.1\omega_H=1.125$, $\delta=0.2$, $L=0.01$, $\sigma=10$, and $\psi=-0.25$.

boundary layers between the convective rolls and close to the plates with large concentration gradients. The fluid is diffusively homogenized in the closed-streamline regions of the rolls leading to anharmonic lateral concentration profiles of trapezoidal shape.

3. TW close to r^{TW}_{min}

The time evolution of the low-frequency modulated TWs close to r^{TW}_{min}, i.e., in the left part of the bifurcation diagram in Fig. 3 is strongly different not only from the TWs that are modulated with a large frequency (Fig. 2, arrows B′ and C′) but also from the TWs that are modulated with low frequency at larger r (Fig. 3, arrows B and C). The differences come from the fact that the driving $r(t)$ stays long enough below the saddle location r^{TW}_S, so that w_{max} decreases to small values in a significant part of the modulation interval.

To elucidate the consequences of this long subcritical intervals we show in Fig. 7 the driving, the mixing number $2M$, w at a fixed location, w_{max}, and the phase velocity v_{ph} of the TW D in Fig. 3—over two modulation periods for better visibility. The latter two velocities and the mixing number oscillate with the period $\tau=2\pi/\Omega$ of the heating $r(t)$. Note the large amplitude oscillations of $v_{ph}(t)$ and the complex variation of w. They show already that the flow dynamics of TW D is significantly more varying and more complex than those of TWs A–C.

The increase in spatiotemporal complexity is even more dramatic for the concentration field of TW D; cf. Fig. 8 with snapshots of C taken at times that are indicated by thick dots in Fig. 7. The reason is that v_{ph} is sometimes larger and sometimes smaller than w or w_{max}. Thus, with the associated advective characteristics open- and closed-streamline regions and with it open and closed isoconcentration lines as they can be seen in TWs under static driving [22,36] for different r's appear here as alternating. This alternation between different mixing regimes in the modulated TW D explains also that the relation of its mixing number $M(t)$ to the actual driving $r(t)$ differs from the one between M and r for stable unmodulated TWs. In the latter M decreases with r as the advective mixing increases [36]. Here, in TW D one sees often the opposite: $M(t)$ increases (decreases) with increasing (decreasing) $r(t)$ since the concentration field does not have time to relax to the instantaneous advective flow. Moreover the strength of the latter is also delayed relative to the thermal driving $r(t)$.

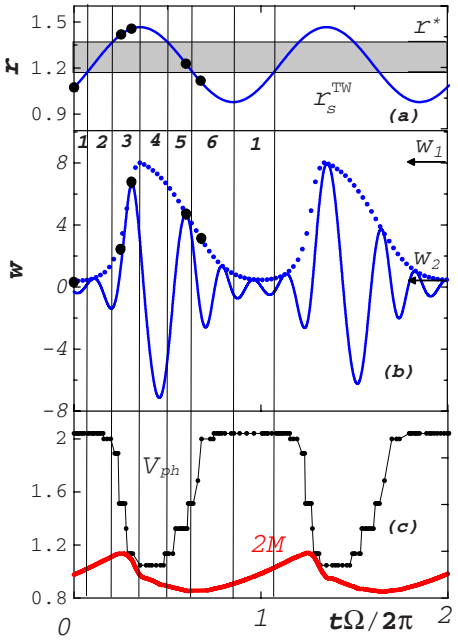

FIG. 7. (Color online) Characteristics of the modulated TW identified by arrow D in Fig. 3 versus time. (a) Variation of $r(t)$. Stable unmodulated TWs exist only in the gray interval between r^{TW}_S and r^*. (b) Full line shows vertical velocity $w(x_0,z=1/2,t)$ at a fixed location, while dotted line shows the maximum $w_{max}(t)$ (2.13) in the whole layer. The oscillation range of the latter is indicated by arrows labeled w_1 and w_2. (c) Thick full line labeled $2M$ refers to twice the mixing number (2.20) of the concentration field. Thin lines with dots show the phase velocity v_{ph}. For better visibility the plots cover two modulation periods. Intervals delimited by thin vertical lines and labeled 1–6 below the abscissa of (a) are discussed in the text. Thick dots in (a) and (b) identify times for snapshots of the concentration distribution shown in Fig. 8. Parameters are $r=1.222$, $\Omega=0.1\omega_H=1.125$, $\delta=0.2$, $L=0.01$, $\sigma=10$, and $\psi=-0.25$.

In order to discuss the spatiotemporal properties of TW D and in particular the structural dynamics of the concentration field in more detail we divide the driving period into intervals I_n $(n=1,\ldots,6)$ delimited by the thin vertical lines in Fig. 7. The boundaries are marked by times at which $r(t)$ reaches characteristic values. So $r(t)$ varies within these intervals between the following values: I_1: $(1-\delta)r\to r^{TW}_S$, I_2: $r^{TW}_S\to r^*$, I_3: $r^*\to(1+\delta)r$, I_4: $(1+\delta)r\to r^*$, I_5: $r^*\to r^{TW}_S$, and I_6: $r^{TW}_S\to(1-\delta)r$.

In the first interval I_1 $r(t)$ increases but the advective velocity w is so small that the thermodiffusive separation strongly influences the system dynamics. Here, concentration gradients and hence $M(t)$ grow following the growth of the

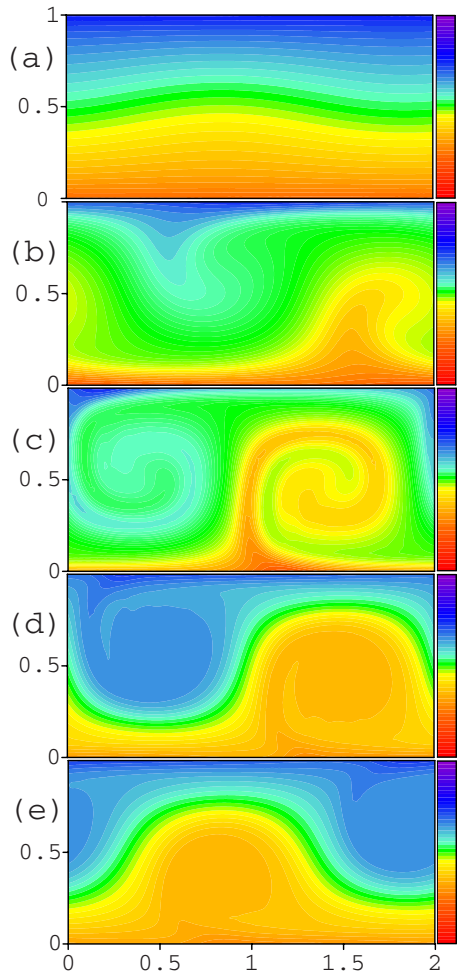

FIG. 8. (Color online) Snapshots of the concentration distribution in the TW at $r=1.222$ (arrow D in Fig. 3) with strong phase and amplitude modulation. The times from top to bottom, $(0,0.254,0.311,0.601,0.679)2\pi/\Omega$ are indicated by thick dots in Fig. 7. The vertical color bars in the color online version show the coding as in Fig. 6. Parameters are $\Omega=0.1\omega_H=1.125$, $\delta=0.2$, $L=0.01$, $\sigma=10$, and $\psi=-0.25$.

applied temperature gradient. In the steady case convective oscillations would decay in the driving intervals I_6, I_1 that lie below r_S^{TW} and the phase velocity and frequency of the decaying TW would increase when approaching the regime of linear damped oscillations close to the conductive state at the particular value of $r<r_S^{TW}<r_{osc}$. But under modulation convection in the intervals I_6, I_1 does not have time enough to decay all the way into the conductive state. Our calculations show that in I_1 the phase velocity is practically constant.

In the second interval I_2 $r(t)$ further increases staying above r_S^{TW}. As in the unmodulated situation ω_{TW} and the phase velocity v_{ph} decrease here with growing $r(t)$. However, the flow velocity w is still small and the advective mixing cannot fully degrade the Soret induced separation, so that M continues to grow. The modulated TWs in the intervals I_1, I_2 are weakly nonlinear with practically harmonic distributions of all fields. All concentration streamlines of these weakly nonlinear TWs are open. Figure 8(a) shows as a representative example the concentration distribution of TW D at time $t=0$ where the advective flow velocity is minimal and the phase velocity is maximal.

In the interval I_3 the advective velocity increases very fast and its maximum w_{max} is larger than about 3, which marks the location of the S-shaped deformation on the unmodulated unstable TW branch [thin dashed line in Fig. 3(a)]. The value of the vertical velocity for which this deformation occurs characterizes the transition from weakly nonlinear to strongly nonlinear TWs with anharmonicities appearing in the concentration field [36]. Figures 8(b) and 8(c) show snapshots of typical concentration distributions appearing in interval I_3 when w_{max} grows into the strongly nonlinear regime in which $w_{max}>v_{ph}$. The TW in Fig. 8(c) has spiral concentration distributions with a large amount of internal boundary layers. From here on the mixing number $M(t)$ abruptly decreases.

At the border between I_3 and I_4 the vertical velocity reaches its maximum equal to the value in the unmodulated SOC state at the largest value $(1+\delta)r$ of $r(t)$ in the modulation cycle. In interval I_4 with $r(t)$ being above the transition at r^* to unmodulated SOC states the advective mixing is very strong, the phase velocity takes on its minimal value, while $M(t)$ continues to decrease.

In I_5 the heating $r(t)$ and with it the advection amplitude decreases while the phase velocity increases again. In the intervals I_4 and I_5 $w_{max}(t)$ follows the driving $r(t)$ practically without phase shift. The TW in Fig. 8(d) that is representative for the interval I_5 shows regions of closed streamlines in the comoving frame. In this left propagating TW the right (left) turning fluid domains are poor (rich) in ethanol and they are displaced toward the upper cold (lower warm) plate, where the Soret effect maintains a boundary layer with alcohol surplus (deficiency) [5].

At the boundary between I_5 and I_6 the vertical velocity reaches the value $w\simeq 4$ which is realized also by the unmodulated TW at its lower existence limit, i.e., the saddle node at r_S^{TW}. Then, in I_6 the thermal driving $r(t)$ falls again below r_S^{TW}. Here, the flow amplitude decreases by a factor of about 10. In the first part of this interval a strongly nonlinear TW is still realized as can be seen from the concentration distribution in Fig. 8(e). But when the advective velocity falls below $w\sim 3$ all isoconcentration lines correspond to a weakly nonlinear TW as in I_1. They are open and the field structures look almost harmonic. Furthermore, the phase velocity reaches its maximum such that $v_{ph}>w_{max}$ which implies weak nonlinearity [36]. Here, thermodiffusive separation plays an important role and the mixing number grows.

4. Modulation with $\Omega=0.01\omega_H$

Here, we show that modulation of the heating with a frequency as small as $\Omega=0.01\omega_H$ causes surprisingly complex convective response when the relative modulation amplitudes are as large as $\delta=0.2$ as in our case. To explain it we show in Fig. 9 the time variation of the mixing number M together with the one, M_{cond}, in the modulated conductive state, the instantaneous frequency ω with which the convective velocity is oscillating, w at a fixed location, and w_{max}. The mean reduced Rayleigh number here is $r=1.227$ which is near the lower end of the existence interval of convection

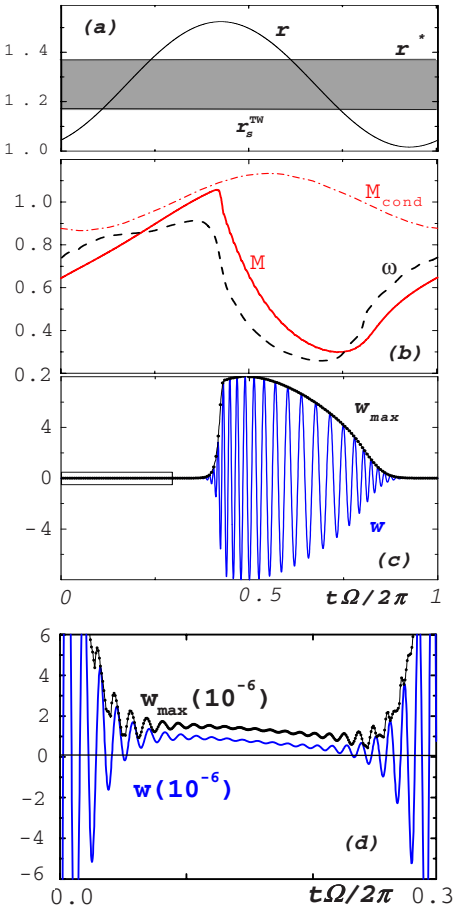

FIG. 9. (Color online) Characteristics of a TW that is modulated with the very low frequency of $\Omega=0.01\omega_H=0.1125$. Here, $r=1.227$ is near the lower end of the existence interval of modulated TWs. (a) Variation of $r(t)$. Stable unmodulated TWs exist only in the gray interval between r_S^{TW} and r^*. (b) Frequency $\omega(t)$, mixing number $M(t)$, and mixing number $M_{cond}(t)$ in the modulated conductive state. (c) Full line shows the vertical velocity $w(x_0,z=1/2,t)$ at a fixed location, while dotted line shows the maximum $w_{max}(t)$ (2.13) in the whole layer. (d) Blowup of a part of (c). Parameters are $\delta=0.2$, $L=0.01$, $\sigma=10$, and $\psi=-0.25$.

modulated with frequency $\Omega=0.01\omega_H$. For this value of r the reduced heating rate $r(t)$ periodically leaves the existence interval (r_S^{TW},r^*) of unmodulated TWs on both sides [cf. Fig. 9(a)]. Some aspects of the behavior of the resulting convection are similar to the previous case of $\Omega=\omega_H/10$. However, there are also significant differences:

(i) In part of the modulation period mixing by advection becomes very small as $w_{max}(t)$ drops down to $\mathcal{O}(10^{-6})$ in Figs. 9(c) and 9(d). Furthermore, since the system has time enough to get very close to the conductive state the behavior during these times can be described within linear theory.

(ii) During the time $0.1\tau<t<0.3\tau$ the phase velocity is zero and convection occurs in the form of a SW with a very small oscillation amplitude. Here, we used the local instantaneous oscillation frequency ω shown in Fig. 9(b) to characterize the convective solution.

(iii) The mixing number M shows a linear growth over almost half the modulation cycle and comes close to the conductive state's value M_{cond} [cf. Fig. 9(b)].

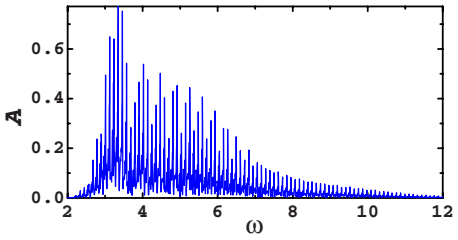

FIG. 10. (Color online) Fourier amplitudes A in arbitrary units in the spectrum of $w(x_0,z=1/2,t)$ versus frequency ω for the TW that is modulated with $\Omega=0.01\omega_H$ at $r=1.227$ (cf. Fig. 9). Parameters are $\delta=0.2$, $L=0.01$, $\sigma=10$, and $\psi=-0.25$.

(iv) In the other part of the modulation period a spikelike behavior of TW activity appears [cf. Fig. 9(c)], that is similar to relaxation oscillations. In the first stage of this activity the advective velocity increases very fast and after that it smoothly relaxes to zero. Simultaneously the mixing number abruptly decreases in the first stage due to the increasing advective mixing.

(v) The frequency $\omega(t)$ in Fig. 9(b) is strongly modulated and shows for our case of slowly modulated heating quite similar behavior as $M(t)$, albeit with some delay between them. To understand this behavior one has to know that for steady heating the size of the Soret induced concentration gradients determines the magnitude of the restoring force for oscillatory convection and that the frequencies of TWs and of SWs obey the relation $\omega/\omega_H\sim M$ (Fig. 3 of Ref. [20]): above r^* the heating has become so large that the advective mixing is strong enough to reduce the Soret induced concentration gradients to effectively zero, so that $\omega=0$ in the SOC state. On the other hand, when moving downward along the unmodulated TW solution branch in Fig. 3(a) all the way to r_{osc}, the flow intensity and with it the advective mixing decrease all the way to zero; the Soret induced concentration gradients and with it the mixing number increase to their maximum value $M=1$ in the quiescent conductive state; and the restoring force for oscillations, i.e., the oscillation frequency, increases to its maximal value ω_H at r_{osc}.

(vi) The temporal Fourier spectrum in Fig. 10 of the TW velocity in Fig. 9 is quasicontinuous. It contains many harmonics and their combinations. The difference between neighboring peaks is the modulation frequency Ω.

C. Fourier dynamics of the flow

To elucidate in detail the spatiotemporal complexity of the different convection solutions considered above we used also the lateral Fourier decomposition (2.19) of velocity, temperature, and concentration in particular at midheight position $z=1/2$. The behavior of the fields there is representative also for other vertical positions. Here, we present results only for the vertical velocity field. In contrast to the concentration field the lateral variation of w is largely harmonic, so that the first Fourier mode $\hat{w}_1$ in representation (2.19) of $w(x,z=1/2,t)$ characterizes the flow behavior.

The trajectory of $\hat{w}_1(t)$ is the projection of the spatiotemporal flow dynamics of the convective state in real space into

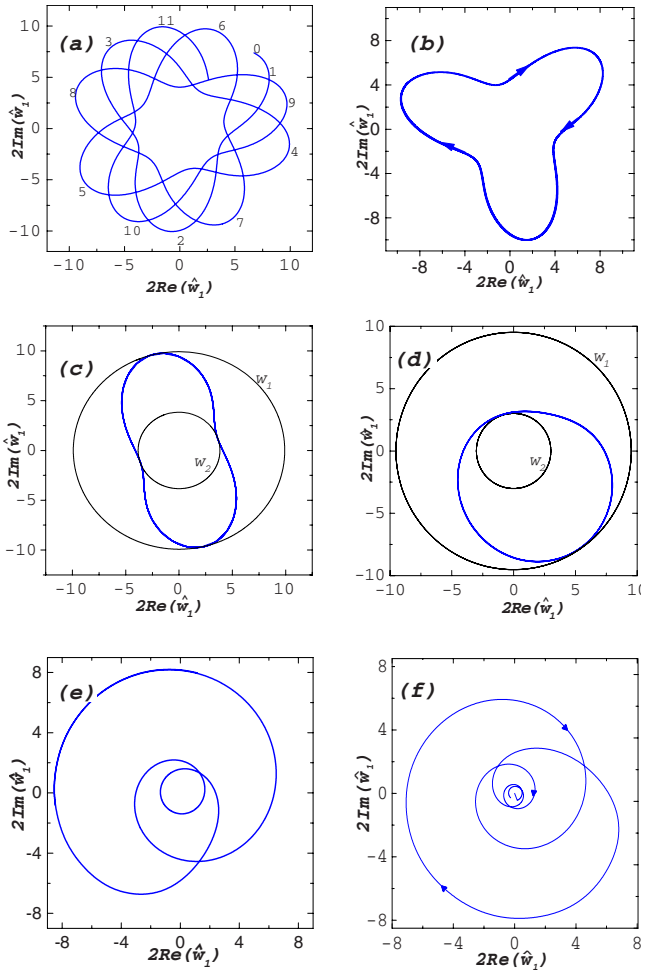

FIG. 11. (Color online) Trajectories of the first lateral Fourier mode $\hat{w}_1(t)$ in the expansion (2.19) of the vertical velocity $w(x_0,z=1/2,t)$ in the plane spanned by the real and imaginary parts of $\hat{w}_1$. (a) Amplitude and phase modulated quasiperiodic TW A with $Q=2.579$ at $r=1.399$, (b) periodic TW with $Q=3$ at $r=1.405$, (c) subharmonic TW with $Q=2$ at $r=1.383$, (d) synchronous TW C with $Q=1$ at $r=1.337$, (e) periodic TW with $Q=1/3$ at $r=1.262$, and (f) strongly modulated quasiperiodic TW D with $Q=0.214$ at $r=1.222$. Parameters are $\Omega=0.1\omega_H=1.125$, $\delta=0.2$, $L=0.01$, $\sigma=10$, and $\psi=-0.25$.

lateral Fourier space. It complements the picture of the TW dynamics of w at a fixed location. In Fig. 11 the time evolution of the complex mode $\hat{w}_1(t)$ is presented in the plane spanned by its real and imaginary parts, respectively, for different convective solutions.

We start our discussion with TW A which is not only amplitude but also phase modulated. Its frequency spectrum is presented in Sec. IV B 1. The trajectory of $\hat{w}_1(t)$ for this TW shown in Fig. 11(a) moves in the annular domain between the two circles of outer radius w_1 and inner radius w_2 that mark the extrema of $w_{max}(t)$ [cf. Fig. 3(a)]. That is so since the field w is very well represented in Eq. (2.19) by the first lateral Fourier mode $\hat{w}_1$.

The time between successive maxima of $|\hat{w}_1(t)|$, i.e., the period of the amplitude modulation is τ, the period of the temperature modulation. At steady heating, $w_1=w_2$, the trajectory in Fig. 11(a) contracts to a circle along which $\hat{w}_1(t)$ would move with constant rotation frequency $\dot{\varphi}_1$ such that $|\dot{\varphi}_1|=\omega_{TW}$.

Left and right propagating TWs being symmetry degenerate—also in the presence of temperature modulation—have oppositely rotating $\hat{w}_1$. The mean frequency $\langle\omega_{TW}\rangle$ (2.17) of our modulated TWs is the mean frequency $\langle|\dot{\varphi}_1|\rangle$ with which the complex number $\hat{w}_1$ rotates in the planes of Fig. 11.

In general the two characteristic frequencies $\langle\omega_{TW}\rangle$ and Ω of the modulated TW are not rationally related to each other. Thus, the TW is quasiperiodic and the trajectory of $\hat{w}_1(t)$ is not closed. The TW A is an example for such a quasiperiodic TW with $Q=\Omega/\omega_{TW}=2.579$. So, here the mean rotation frequency $\langle\omega_{TW}\rangle=\langle|\dot{\varphi}_1|\rangle$ of $\hat{w}_1$ is by a factor of 2.579 smaller than the oscillation frequency of its modulus $|\hat{w}_1|$. In Fig. 11(a) we show the trajectory over 11 periods of the modulation. Thus, during this time $\hat{w}_1(t)$ moves 11 times from the outer circular boundary of the annular domain at radius w_1 to the inner one at radius w_2 and back. For the convenience of the reader we have indicated the start by 0. Consecutive maxima of $|\hat{w}_1|$ are numbered from 1 to 11.

In Figs. 11(b)–11(d) we show the trajectories for periodic TWs with $Q=3$, 2, and 1, respectively. Here, the orbits of $\hat{w}_1(t)$ are closed after three, two, and one period of $r(t)$, respectively. Like the one in Fig. 11(a) they can be well approximated by the simple formulas for $|\hat{w}_1(t)|$ (4.2b) and for $\varphi_1(t)$ (4.2c). In these TWs the phase velocity is significantly modulated such that $|\dot{\varphi}_1|$ is large when $|\hat{w}_1|$ is small.

The trajectory in Fig. 11(b) belongs to a TW at $r=1.405$ with a mean frequency $\langle\omega_{TW}\rangle=\Omega/3$ that is slightly smaller than the one of TW A shown in Fig. 11(a). The subharmonically responding TW B at $r=1.383$ that is shown in Fig. 11(c) has with $\langle\omega_{TW}\rangle=\Omega/2$ a frequency that is larger than that of TW A since according to Fig. 3(b) $\langle\omega_{TW}\rangle$ increases with decreasing r. For the synchronous TW C in Fig. 11(d) at $r=1.337$ one has $\langle\omega_{TW}\rangle=\Omega$. Its trajectory with its center being displaced from the origin has less symmetry than the ones for $Q=2$ and 3. This explains with representation (4.2) that the synchronous TW with $Q=1$ does not display the time-shift symmetry (4.3) (cf. Sec. IV B 2).

Figure 11(e) shows an example of the periodic motion of $\hat{w}_1(t)$ for a TW with $Q=1/m$; here, $Q=1/3$. The trajectory is closed after the time τ, i.e., after one period of $r(t)$. This is also the periodicity of the convective response. The mean TW frequency $\langle\omega_{TW}\rangle$, on the other hand, is defined via the long-time average of the velocity of the nodes of, say, $w(x,z=1/2,t)=|\hat{w}_1(t)|\cos[\varphi(t)-kx]$ according to Eqs. (2.16) and (2.17). Here, this quantity is three times larger than Ω since the rate of change $\dot{\varphi}_1$ of the phase in Fig. 11(e) is on average three times larger than Ω. The asymmetry of the trajectory of $\hat{w}_1(t)$ implies also here like in the case for $Q=1$ in Fig. 11(d) that the time average of the vertical velocity is nonzero, giving rise to a stationary laterally periodic contribution.

Figure 11(f) shows the motion of $\hat{w}_1(t)$ for the strongly amplitude and phase modulated TW D with $Q=0.214$. Here, $w_2\simeq 0.3$ and $w_1\simeq 8$.

D. Harmonic response with fixed spatial phase

When the mean heating rate is increased the mean TW frequency $\langle\omega_{TW}\rangle$ decreases as in the absence of modulation. Thus, the peaks in the Fourier spectrum of Fig. 4(a) at $\Omega\pm\langle\omega_{TW}\rangle$ approach each other as indicated by the dotted horizontal arrows in Fig. 4(a). At $r=1.430$ the TW frequency $\langle\omega_{TW}\rangle$ drops to zero [cf. Fig. 3(b)]. Beyond this r value, convective solutions with a fixed spatial phase are realized to be oscillating synchronously with $r(t)$: in the regime marked as MC in Fig. 3 only one main peak remains in the Fourier spectrum of $w(x_0,z=1/2,t)$ that is located at the imposed modulation frequency Ω plus higher harmonics thereof.

In this MC regime, the flow basically just oscillates around the unmodulated SOC state's flow. Also the mean of $w_{max}(t)$ (2.13) is practically given by w_{max} in the SOC state for stationary driving: the thin line in Fig. 3(a) lies in the middle between the thick lines for w_1 and w_2.

Furthermore, one observes also for modulated heating the $\delta=0$ scenario for the transition from TWs to SOCs: the phase velocity decreases with increasing r since advection increases. Thereby the regions of closed streamlines grow at the expense of the open ones. Consequently, the former also come closer to the respective opposing horizontal boundary layers. This decreases the asymmetry of the boundary layer feeding into oppositely turning rolls. As a consequence, the concentration contrast between adjacent TW rolls—which drives the lateral phase propagation of the TWs—decreases until in the MC state with $v_{ph}=0$ the oppositely turning rolls are fed symmetrically by both boundary layers.

The concentration field in the MC solution looks like the one in SOC states for stationary driving [20] with the advective mixing being much stronger than in TWs. The qualitative behavior of the concentration field in the MC state is also the same as for modulation with larger frequencies [24]. However, for our low-frequency modulation the concentration distribution is more homogeneous at the maximum of the vertical velocity (M is smaller) and when w is minimal the boundary layers near the two plates are more pronounced.

Finally, we note that the end of the modulated TW solution branch and the beginning of the MC regime are shifted to larger r when the modulation frequency Ω decreases. The reason is that with decreasing Ω the concentration difference between top and bottom plates increases as shown in Fig. 1. Thus, it is necessary to apply a larger r causing a larger advection to mix the binary fluid.

V. CONCLUSION

The bifurcation properties and the spatiotemporal behavior of oscillating convection rolls in binary fluid mixtures subject to low-frequency harmonic modulation of the bottom boundary's temperature were investigated in a cross section perpendicular to the roll axes. Finite difference numerical simulations were performed for parameters adapted to experiments that use ethanol-water mixtures with sufficiently negative Soret coupling to show subcritical Hopf bifurcations into SWs and TWs. Various visualization and diagnostic tools were used to elucidate the spatiotemporal structure and bifurcation properties of the rich and rather complex strongly nonlinear response behavior to the modulation of the thermal driving.

Quasiperiodic as well as different periodic modulated traveling waves and synchronously modulated patterns with a fixed spatial phase (MC) are found as stable solutions. The full bifurcation behavior of TWs and MCs has been presented and their typical temporal oscillations, frequency properties, and concentration field structures are discussed in detail. It is shown that low-frequency modulation shifts the lower and upper ends of the existence interval of TW convection to larger mean Rayleigh numbers in comparison to stationary heating. Under temperature modulation the buoyancy-induced advection gets modulated and leads in particular for the modulated TWs to complex nonlinear mixing behavior. The symmetry properties of the various periodic TWs are discussed. It is shown that contrary to the case of large-frequency modulation [24] a stable SW solution does not exist under low-frequency heating. Anomalous variations of the mixing number relative to the magnitude of the advective velocity are observed and explained. Peculiarities of the response to very low frequencies are discussed when the heating remains for a long time below the saddle Rayleigh number of the backward bifurcating TW under stationary heating.

ACKNOWLEDGMENTS

This work was supported by the Deutsche Forschungsgemeinschaft in the framework of GRK 1276 "Strukturbildung und Transport in komplexen Systemen."

[1] M. C. Cross and P. C. Hohenberg, Rev. Mod. Phys. **65**, 851 (1993).

[2] For 5 wt % of ethanol mixed into water at $T=20$ °C the separation ratio measuring the Soret coupling strength [1] is $\psi\simeq -0.3$ [3].

[3] P. Kolodner, H. L. Williams, and C. Moe, J. Chem. Phys. **88**, 6512 (1988).

[4] R. W. Walden, P. Kolodner, A. Passner, and C. M. Surko, Phys. Rev. Lett. **55**, 496 (1985).

[5] M. Lücke, W. Barten, P. Büchel, C. Fütterer, St. Hollinger, and Ch. Jung, in *Evolution of Structures in Dissipative Continuous Systems*, Lecture Notes in Physics Vol. m55, edited by F. H. Busse and S. C. Müller (Springer, Berlin, 1998), p. 127.

[6] E. Moses, J. Fineberg, and V. Steinberg, Phys. Rev. A **35**, 2757 (1987); R. Heinrichs, G. Ahlers, and D. S. Cannell, *ibid.* **35**, 2761 (1987).

[7] K. E. Anderson and R. P. Behringer, Phys. Lett. A **145**, 323 (1990); Physica D **51**, 444 (1991).

[8] B. I. Winkler and P. Kolodner, J. Fluid Mech. **240**, 31 (1992).
[9] P. Kolodner, Phys. Rev. E **50**, 2731 (1994).
[10] H. Touiri, J. K. Platten, and G. Chavepeyer, Eur. J. Mech. B/Fluids **15**, 241 (1996).
[11] E. Kaplan, E. Kuznetsov, and V. Steinberg, Phys. Rev. E **50**, 3712 (1994).
[12] C. M. Surko, D. R. Ohlsen, S. Y. Yamamoto, and P. Kolodner, Phys. Rev. A **43**, 7101 (1991).
[13] C. M. Aegerter and C. M. Surko, Phys. Rev. E **63**, 046301 (2001).
[14] L. Ning, Y. Harada, and H. Yahata, Prog. Theor. Phys. **98**, 551 (1997).
[15] O. Batiste, E. Knobloch, I. Mercader, and M. Net, Phys. Rev. E **65**, 016303 (2001).
[16] D. Jung and M. Lücke, Phys. Rev. Lett. **89**, 054502 (2002); Phys. Rev. E **72**, 026307 (2005).
[17] D. Bensimon, P. Kolodner, C. M. Surko, H. Williams, and V. Croquette, J. Fluid Mech. **217**, 441 (1990).
[18] P. Kolodner, Phys. Rev. A **46**, 6452 (1992).
[19] P. Matura, D. Jung, and M. Lücke, Phys. Rev. Lett. **92**, 254501 (2004).
[20] D. Jung, P. Matura, and M. Lücke, Eur. Phys. J. E **15**, 293 (2004).
[21] W. Barten, M. Lücke, M. Kamps, and R. Schmitz, Phys. Rev. E **51**, 5636 (1995); **51**, 5662 (1995).
[22] C. Fütterer and M. Lücke, Phys. Rev. E **65**, 036315 (2002).
[23] M. I. Shliomis and B. L. Smorodin, Phys. Rev. E **71**, 036312 (2005).
[24] B. L. Smorodin and M. Lücke, Phys. Rev. E **79**, 026315 (2009).
[25] B. L. Smorodin, B. I. Myznikova, and J. C. Legros, Phys. Fluids **20**, 094102 (2008).
[26] G. Z. Gershuni and E. M. Zhukhovitsky, *Convective Stability of Incompressible Fluids* (Keter, Jerusalem, 1976).
[27] G. Venezian, J. Fluid Mech. **35**, 243 (1969).
[28] S. Rosenblat and G. A. Tanaka, Phys. Fluids **14**, 1319 (1971).
[29] C.-S. Yih and C.-H. Li, J. Fluid Mech. **54**, 143 (1972).
[30] G. Ahlers, P. C. Hohenberg, and M. Lücke, Phys. Rev. A **32**, 3519 (1985).
[31] G. Ahlers, P. C. Hohenberg, and M. Lücke, Phys. Rev. A **32**, 3493 (1985).
[32] A. Alonso and O. Batiste, Theor. Comput. Fluid Dyn. **18**, 239 (2004).
[33] L. D. Landau and E. M. Lifschitz, *Course of Theoretical Physics* (Pergamon Press, Oxford, 1993), Vol. 6.
[34] J. K. Platten and J. C. Legros, *Convection in Liquids* (Springer, Berlin, 1984).
[35] St. Hollinger and M. Lücke, Phys. Rev. E **57**, 4238 (1998).
[36] St. Hollinger, P. Büchel, and M. Lücke, Phys. Rev. Lett. **78**, 235 (1997).